DØ Note 5746-CONF

Measurement of Top Quark Mass in Dilepton Final States via Neutrino Weighting

DØ Collaboration
URL http://www-d0.fnal.gov
(Dated: July 27, 2008)

As the heaviest known fundamental particle, the top quark is a unique probe of the physics of electroweak symmetry breaking. This paper presents new results in 1 fb^{-1} of Tevatron data as measured by the DØ experiment. Decays of $t\bar{t}$ into $\ell\bar{\ell}' + \nu\bar{\nu}' + b\bar{b}$ states are analyzed with one selection requiring two fully identified leptons ($\ell = e, \mu$), and a second selection relaxing one lepton requirement but adding a secondary vertex $b-$tag. Events are kinematically reconstructed by integrating over expected neutrino rapidity distributions. Mass estimators for each event are derived as the first two moments of resulting per-event weight distributions. The top quark mass (m_t) is extracted from 82 candidate events in data by an unbinned maximum likelihood method to give $m_t = 176.0 \pm 5.3(\text{stat}) \pm 2.0(\text{sys})$ GeV. The dominant systematic uncertainty comes from the jet energy calibration.

I. INTRODUCTION

When the top quark was discovered in 1995 [1, 2], emphasis quickly turned to the measurement of its mass across all its reconstructable final states. The reasons for this emphasis are manifold. As the heaviest fundamental particle known, a measurement of m_t is a unique probe of electroweak symmetry breaking. In fact, m_t and the value of the Higgs boson mass, M_H, can be related by radiative corrections to the W boson mass, M_W. One loop corrections give $M_W^2 = \frac{\pi\alpha/\sqrt{2}G_F}{sin^2\theta_W(1-\Delta r)}$ where Δr includes a dependence on the value of m_t: $\frac{3G_F m_t^2}{8\sqrt{2}\pi^2 tan^2\theta_w}$, and on the Higgs mass ($\frac{11G_F M_Z^2\cos^2\theta_W}{24\sqrt{2}\pi^2}\ln\frac{M_H^2}{M_Z^2}$).

Beyond its relation to M_H, the top quark mass reflects the Yukawa coupling, Y_t, for the top quark via $Y_t \sim m_t\sqrt{2}/v$ where v is the vacuum expectation value. Given that these couplings are not predicted by the theory, Y_t is curiously close to unity. One of several possible modifications to the mechanism underlying electroweak symmetry breaking might be responsible. For instance, the top quark itself may play a major role via topcolor-assisted technicolor [3], [4]. These models entirely remove the need for a scalar Higgs field in favor of new strong interactions which provide the observed mass spectrum. Perhaps there are extra Higgs doublets as in MSSM models [5]. Measurement of the top quark mass may provide a useful indicator of such models (e.g. Ref. [6]).

We can measure m_t in $t\bar{t}$ events with dilepton final states. In the absence of new fermion families or additional charged bosons, $BR(t \to Wb)$ is expected to be nearly 100%. So the rates of top quark final states are dictated by the branching ratios of the W bosons to various fermion pairs. Approximately 10% of $t\bar{t}$ events have both W bosons decaying leptonically. Generally, only the $e\nu$ and $\mu\nu$ modes yield clean, well calibrated channels that can readily be used for mass analysis. Interesting channels involve the presence of two e's, two μ's or an $e\mu$ pair. These channels provide an important independent statistical sample with which to measure m_t. The systematic effects on such a measurement also comprises a different set than in other $t\bar{t}$ final states. This is true partly because fewer jets are present, and also because backgrounds come from a different array of processes.

Previous efforts to measure m_t in the dilepton channel have involved several techniques, many of which fall into the category of template-based methods. An underconstrained fit results from two neutrinos in each event. A solution is obtained by assuming a range of input top quark masses and calculating the consistency of the observed kinematics with each. Events can then be weighted based on input parton distribution functions and lepton energies[10]. This 'matrix weighting' or MWT approach has been used with Run I data of the Tevatron [11]. One can also integrate over expected neutrino rapidity distributions (νWT) to obtain a relative probability per tested top quark mass, as was also done in Run I [11]. We have pursued both approaches using 370 pb^{-1} of Run II Tevatron data [12]. CDF has adopted the νWT approach in 192 pb^{-1} [13]. Both Run I analyses used a multi-parameter probability density technique to extract a measure of m_t. The Run II MWT and CDF analyses have used single parameter fits.

The current paper describes a measurement of the top quark mass in 1 fb^{-1} of $p\bar{p}$ collider data using the νWT approach. Events with two explicitly identified leptons, termed '2ℓ', are analyzed. $b-$tagged events with one explicit lepton (e or μ) and an isolated high p_T track (an implicit lepton) are also included; these being labeled 'ℓ+track' events. The method of mass estimation for the νWT analysis is modified from earlier efforts by a simpler use of the moments of the weight distribution to get the full benefit of the information contained about m_t. We describe in the next two sections the detector and the event reconstruction, as well as the data samples gathered with the DØ detector and used in this analysis. Subsequent sections describe the modeling of signal and background and its validation with the DØ data sample. The kinematic reconstruction and maximum likelihood analysis to extract a measure of m_t are discussed. The statistical validation of our approach is followed by discussion of final results and systematic uncertainties.

II. DETECTOR AND DATA SAMPLE

A. Detector Components

The DØ Run II detector [21] is a multipurpose collider detector consisting of an innermost magnetic central tracking system, a calorimetry system and outer muon tracking detectors. The spatial coordinates of the DØ detector are defined as follows: the positive z direction is along the direction of the proton motion while positive y is defined as upward from the detector's center, which serves as the origin. The polar angle θ is measured with respect to the positive z direction and is usually expressed as the pseudorapidity, $\eta \equiv -\ln(\tan(\theta/2))$. The azimuthal angle ϕ is measured with respect to the positive x direction, which points to the center of the Tevatron ring.

The tracking detectors are responsible for measuring the trajectories and momenta of charged particles and locating the event primary vertex. They reside inside a 2T superconducting solenoid. A silicon microstrip tracker (SMT)

provides precision position measurements, particularly in the azimuthal plane, which allow the location of displaced, secondary vertices from the decay of long-lived particles. This permits identification of jets from heavy flavor quarks, particularly b quarks, to $|\eta| \approx 3.0$. A central fiber tracker (CFT) is composed of scintillator fibers mounted on eight concentric support cylinders. Each cylinder supports axial and stereo layers of fibers, alternating by $\pm 3^\circ$ relative to the cylinder axis. The outermost cylinder provides coverage for $|\eta| < 1.7$.

Calorimetry measures $e^\pm$ and jet energies, directions and shower parameters relevant for particle identification. Neutrinos are also measured via the calorimeters' hermeticity and the constraint of momentum conservation in the plane transverse to the beam direction. Three liquid Ar filled cryostats containing uranium absorbers constitute the central (CC) and endcap (EC) calorimeter systems. The CC covers $|\eta| < 1.1$, and the endcaps extend coverage to $|\eta| < 4.2$. Each calorimeter consists of an electromagnetic (EM) section followed by fine and coarse thickness hadronic sections. Readout cells are arrayed in a projective geometry with respect to the nominal interaction region.

Drift tubes and scintillators are arranged in planes on all sides of the calorimeter system to measure the trajectories of penetrating muons. One drift tube layer resides inside a 1.8 T iron toroid, while two more layers are outside. The cumulative coverage of the drift tubes is $|\eta| < 2$.

B. Data Sample

Trigger and data acquisition systems are designed to accommodate luminosities of 2×10^{32}. The luminosity measurement is based on the rate of inelastic $p\bar{p}$ collisions observed by plastic scintillation counters mounted on the inwardly directed faces of the calorimeter endcap cryostats. Based on preliminary information from tracking, calorimetry, and muon systems, the output of the first level of the trigger is used to limit the rate for accepted events to approximately 2 kHz. At the next trigger stage, with more refined information, the rate is reduced further to about 1 kHz. These first two levels of triggering rely mainly on hardware and firmware. The third level software trigger reconstructs all of the event information to reduce the output rate to about 50 Hz, which is written to tape.

Several different triggers were used for the five channels analyzed for this paper. Triggers requiring one e and one μ were used for the $e\mu$ channel. Single electron triggers were used for $e\mu$, ee and e+track channels, while single μ triggers were used for $e\mu$, $\mu\mu$ and μ+track channels. Additional triggers requiring one e or μ plus a single jet were used for the e+track and μ+track channels, respectively. Events were collected with these triggers at DØ between April 2002 and February 2007 of Run II at the Tevatron. Data quality selection removes events where the tracker, calorimeter and muon systems are known to be functioning improperly. The analyzed data sample is 1 fb^{-1}.

C. Event Reconstruction

The event primary vertex, PV, is identified by ≥ 3 associated charged particle tracks. We require $|z_{PV}| < 60$ cm.

Electrons are identified when EM layer calorimeter cells are clustered according to a $\Delta\mathcal{R}(=\sqrt{\Delta\eta^2+\Delta\phi^2}) < 0.2$ cone algorithm and then found to match an inner detector track. The clusters must have the fraction of their energy, f_{EM}, in EM layers to be at least 90 %, must satisfy an $H-$matrix [8] shower shape test that $\chi^2_{hmx} < 50$ with respect to electron showers. The matching track must have $p_T^{trk} > 5$ GeV. Isolated electrons are selected when the nearby calorimeter energy totals < 15 % of the cluster E_T^{clus}. To further remove backgrounds, a likelihood is calculated based on 7 input parameters: E_T^{clus}/p_T^{trk}, χ^2_{hmx}, f_{EM}, χ^2 of the spatial track match, d_{CA} of the track, the distance $\Delta\mathcal{R}$ to the second closest track to the EM cluster, and a track isolation calculated as the sum of track p_T's in a halo from $0.05 < \Delta R < 0.4$ around the electron. A cut on the likelihood of > 0.85 is applied. The final electron energy calibration is determined by precise comparison of the invariant mass of high p_T electron pairs with the world average value of the Z boson mass as measured by the LEP experiments [14].

Muons are identified by tracks reconstructed in the muon system which match a track in the inner tracking system. The following conditions are applied to the inner tracks: $\chi^2_{trk} < 4$ with respect to a circular trajectory, and the distance of closest approach (d_{CA}) of the track with respect to the primary vertex is < 0.02 (< 0.2) cm for tracks with (without) SMT hits. Isolated muons are identified by their separation from calorimeter jets, $\Delta\mathcal{R}(jet,\mu) > 0.5$, and by requiring the sum of charged track momenta in a cone around the muon track to be < 0.15 of the muon p_T. The distance between the selected muon z at transverse radius of zero and the primary vertex, $|z_{muon} - z_{PV}|$, must be < 1 cm.

A partially identified lepton for use in the ℓ+track channels is specified as an isolated track. The track satisfies the same quality and isolation criteria as applied to tracks matching identified muons. Additionally, it must have a d_{CA} significance $d_{CA}/\sigma_{d_{CA}} < 2.5$, and the track isolation is tightened to < 0.1. Double-counting leptons is avoided by $\Delta R(track,\ell) > 0.5$. In events with muons, the distance of the track z intercept should be < 1 cm from that of the corresponding muon track.

Jets are reconstructed with a fixed cone algorithm [9] with radius $\Delta\mathcal{R} < 0.5$. The energy of a jet is measured as the sum of energies deposited in calorimeter cells inside of this cone. The standard jet selection includes the following cuts: the jet EM energy fraction is in the range 0.05 to 0.95, the jet coarse hadronic fraction is less than 0.4. Additionally, jets are required to be confirmed by the electronically independent Level 1 calorimeter trigger readout chain.

Because the $b-$jets carry away much of the energy from the initial top quark's mass, it is critical that jet energies be well calibrated for a mass measurement. Jet energies determined from the event reconstruction do not initially correspond to the energies of final state particles striking the calorimeter. As a result, a detailed *in situ* calibration is applied. In general, the energy of the final state particles of the jet, E_j^{ptcl}, can be related to the measured jet energy, E_j^{meas} by $E_j^{ptcl} = \frac{E_j^{meas} - O}{R_j S_j}$. O, R_j and S_j denote an offset energy primarily from extra interactions in or out of time with an event, the cumulative response of jet particles, and the net energy losses from a jet due to showering, respectively. For a given cone radius, O and S_j are functions of the η within the detector. O is also a function of the number of reconstructed event vertices and the instantaneous luminosity. R_j is the largest correction and reflects the effects of somewhat lower response of the calorimeters to charged hadrons relative to electrons and photons. It also includes the impact of energy losses in front of the calorimeter. The primary response correction is derived from γ+jet events and has substantial dependences on jet energy and η. For all jets which contain a non-isolated muon, the p_T of the muon is added to that of the jet. It is worth noting that the correction procedure here does not correct all the way back to the original b quark parton energy. We will revisit this issue in Section IV when discussing signal and background modeling.

The b-quark jets are tagged using a neural network b-jet tagging algorithm. This combines the impact parameters for all tracks in a jet, as well as information about reconstructed secondary vertices in the jet. Secondary vertices are reconstructed from two or more tracks satisfying: $p_T > 1$ GeV, more than one hit in the SMT, and impact parameter significance $d_{CA}/\sigma_{d_{CA}} > 3.5$. Tracks identified as arising from K_S^0 or Λ decay or from γ conversions are not used for secondary vertex reconstruction. For a mis-tag rate of 0.95 % for light quark jets, we obtain a typical tag rate of 54 % in data for b jets with $|\eta| < 2.4$.

The $\not\!\!E_T$ is equal in magnitude and opposite in direction to the vector sum of all significant calorimeter cell transverse energies. It is corrected for the transverse momenta of all isolated muons, as well as for the *in situ* corrections to the electron and jet energies. A more detailed description of the object reconstruction can be found in [22].

III. EVENT SELECTION

Events are selected for all channels that have two leptons (2ℓ) or a lepton and isolated track (ℓ+track) each with $p_T > 15$ GeV. Electrons must be within $|\eta| < 1.1$ or $1.5 < |\eta| < 2.5$, while muons should have $|\eta| < 2.0$. An opposite sign requirement is applied to the two isolated leptons or lepton and track. Two jets are also required to have pseudorapidity of $|\eta| < 2.5$ and p_T of at least 20 GeV. Since neutrinos coming from W boson decay in $t\bar{t}$ events are a source of significant missing energy, a cut on $\not\!\!E_T$ is a powerful discriminant against background processes without neutrinos such as $Z/\gamma^* \to ee$ and $Z/\gamma^* \to \mu\mu$. Aside from the $e\mu$ channel, all events must have at least $\not\!\!E_T > 25$ GeV.

A. 2ℓ-specific Selection

The e and μ momentum resolutions are quite different. Also, the $e\mu$ channel has a different balance of backgrounds than the other 2ℓ channels which have like-flavored dilepton resonance production of Z bosons. For these reasons, significant differences in event selection are used across all of the dilepton channels.

In the ee channel events with a two electron invariant mass (M_{ee}) of < 15 GeV or $80 < M_{ee} < 100$ GeV are rejected. $\not\!\!E_T$ cuts of $\not\!\!E_T > 35$ GeV and $\not\!\!E_T > 40$ GeV are required when $M_{ee} > 100$ GeV and $15 < M_{ee} < 80$ GeV respectively. In the $\mu\mu$ channel, events with $\not\!\!E_T > 40$ GeV are selected.

In the $e\mu$ analysis no cut on $\not\!\!E_T$ is applied due to the fact that the final states for the main background process $Z/\gamma^* \to \tau\tau$ contain two tau leptons. Their decay products include neutrinos with moderate p_T, and this reduces the effectiveness of a $\not\!\!E_T$ cut on this background. Instead, the final selection in this channel requires H_T, defined as $H_T^i = p_T^{l_1} + \Sigma(p_T^j)$, to be greater than 115 GeV, where $p_T^{l_1}$ denotes the transverse momentum of the leading lepton. This requirement rejects the largest backgrounds for this final state, which arise from $Z/\gamma^* \to \tau^+\tau^-$ and diboson production. The H_T selection is particularly effective in the $e\mu$ channel because of the absence of the $\not\!\!E_T$ cut.

The final selection in the ee channel requires sphericity $\mathcal{S}$ to be greater than 0.15. The sphericity is defined as: $\mathcal{S} = \frac{3}{2}(\epsilon_1 + \epsilon_2)$ where ϵ_1 and ϵ_2 are the two eigenvalues of the normalized momentum tensor of the event. The tensor M_{xy} is calculated as $M_{xy} = \frac{\sum_i p_x^i p_y^i}{\sum_i (p^i)^2}$. This requirement rejects events in which jets are produced in a planar geometry,

which is typical for the background processes.

The final selection applied in the $\mu^+\mu^-$ channel does not impose any cut on $\mathcal{S}$ due to worse μ momentum resolution, but rejects the $Z/\gamma^* \to \mu^+\mu^-$ background by requiring a cut of > 5 on $\not\!\!E_T$ significance likelihood. This quantity is calculated as the log of the probability for the event's measured $\not\!\!E_T$ to arise from the resolutions of the measured μ's.

We selected 39 events in the $e\mu$ channel, 17 events in the ee channel and 13 events in the $\mu\mu$ channel.

B. ℓ+track-specific Selection

The dominant ℓ+track background arises from $Z \to ee$ and $Z \to \mu\mu$ production, so we design the event selection to reject these events. For the e+track channel, electrons are further restricted to $|\eta| < 1.1$, and the leading jet must have $p_T > 40$ GeV. A lepton-track invariant mass, $M_{\ell t}$, window is defined to be $70 < M_{\ell t} < 110$ GeV. The $\not\!\!E_T$ requirement is tightened to $\not\!\!E_T > 35$ GeV inside this window for the e+track channel, and to $\not\!\!E_T > 40$ GeV inside this window for the μ+track channel. Furthermore, a variable $\not\!\!E_T^{Z-fit}$ was designed to compensate for events with mismeasured $\not\!\!E_T$ in the Z background processes. We rescale the lepton and track momenta to bring the invariant mass of the ℓ+track system to the mass of the Z boson (91.2 GeV) and then use these rescaled momenta to correct the $\not\!\!E_T$. This is particularly useful if at least one of the lepton momenta is measured with tracking as opposed to calorimetry, as in the ℓ+track channels. The cuts on $\not\!\!E_T^{Z-fit}$ are identical to those on $\not\!\!E_T$.

A secondary vertex detached in the transverse plane from the event primary vertex provides a powerful discriminant against background, which unlike $t\bar{t}$ have a low heavy flavor jet content. At least one jet is required to be identified as a $b-$jet by the algorithm described in Section II C.

The additional cuts on $\not\!\!E_T$ $\not\!\!E_T^{Z-fit}$, and the b tagging in this analysis were chosen to give the best expected statistical uncertainty in the m_t measurement in the following way. For each set of $\not\!\!E_T$ and $\not\!\!E_T^{Z-fit}$ cuts a set of ensemble tests was performed and the average value of statistical uncertainty was recorded. The expected statistical uncertainty smoothly varied over a 15% range, and we chose the optimal minimum. This study was sensitive to 5% changes of the average statistical error. There was no visible improvement in statistical error when optimizing the 2ℓ channel selection relative to the starting point used for the $t\bar{t}$ cross section analysis.

We selected 8 events in the e+track channel and 6 events in the μ+track channel.

IV. MODELING SIGNAL AND BACKGROUND

An accurate description of the composition of the selected data samples is essential to the mass measurement. In addition, the kinematic description of the $t\bar{t}$ and background is important. The assumption that all $t\bar{t}$ events in our samples adhere to Standard Model production and decay, and that our background levels are correct, are tested in the CDF [15] and DØ [16] cross section measurements. These analyses also revealed consistency of observed data samples with simulated expectations across a wide range of kinematic parameters. In this section, we outline the modeling of signal and background processes, with some emphasis on the ℓ+track analysis which is unique to the measurement presented here..

A. Signal and Background Simulation

Monte Carlo samples for the $t\bar{t}$ processes are generated for ten values of the top quark mass between 155 and 200 GeV. The event generation, fragmentation and decay are performed by Pythia[17] $v6\_319$. Background processes are termed 'physics' backgrounds when charged leptons originate from heavy boson decay and when $\not\!\!E_T$ comes from high p_T neutrinos. This includes $Z/\gamma^* \to \tau\tau$ with $\tau \to e, \mu$ and diboson production WW/WZ. The $Z/\gamma^* \to \tau\tau$ background processes are generated with Alpgen [18] 2.11 as the event generator and Pythia for fragmentation and decay. To avoid double counting of the QCD processes between the two generators, the exact jet-parton matching scheme [19] is employed in Alpgen. The WW/WZ background processes are simulated with Pythia. The parton distribution function is CTE6QL1. Geant3 [20] is used for the detector simulation.

In order to ensure that reconstructed quantities in these samples reflect the performance of the detector in data, several corrections were applied. The Monte Carlo was reweighted by luminosity and beamshape to match the profile in data. Z boson samples were reweighted to the observed distribution of p_T^Z.

Differences between data and Monte Carlo in the efficiency to find leptons, isolated tracks and jets are folded into the Monte Carlo event samples. These corrections are p_T and η dependent scale factors. Jet and lepton p_T resolutions are adjusted to reflect the data performance. Monte Carlo ℓ+track events are weighted according to the probability

that they would pass the $b-$tag cut. This probability is defined as:

$$P = 1 - \prod_{i=1}^{N_{jets}} (1 - p_i(\eta, p_T, \text{flavor}) \tag{1}$$

where $p_i(\eta, p_T, \text{flavor})$ is the probability of i^{th} jet to be identified as a jet originating from b quark. This product is taken over all jets.

The jet energy scale for DØ is determined separately for data and for Monte Carlo jets. The difference in correction is taken as a final adjustment to Monte Carlo jets. This adjustment was then propagated into the event $\not\!\!E_T$. Both mass analyses in this paper use a template calibration procedure to connect the reconstructed top quark mass to an input value of m_t. Therefore, we do not explicitly apply corrections designed to bring jet energies into agreement with the initial b quark momenta. Instead, we employ transfer functions which reflect the relation between final jet and initial b quark kinematics when we do the kinematic reconstruction per event, as described in Section V.

B. Instrumental Backgrounds

Backgrounds can arise from instrumental effects in which $\not\!\!E_T$ is mismeasured. The main instrumental background for the ee, $\mu\mu$, $e + track$ and $\mu + track$ channels are the $Z/\gamma^* \to ee$ and $Z/\gamma^* \to \mu\mu$ processes. In these cases, apparent $\not\!\!E_T$ results from tails in jet or lepton p_T resolutions. For the ℓ+track and $\mu\mu$ channels, event yields for such processes are obtained from data by using the selected Z/γ^* candidate sample in data to normalize the Monte Carlo distribution. In the ee channel, we determine the probability that processes without real high p_T neutrinos pass the $\not\!\!E_T$ selection by measuring the ratio of the number of events above and below a particular $\not\!\!E_T$ threshold in $\gamma + 2$ jets candidate events. This sample is observed to have the same $\not\!\!E_T$ distribution as $Z/\gamma^* \to ee$ Monte Carlo. This probability is multiplied by the number of data events that fail the $\not\!\!E_T$ selections but pass all other selections to get the number of fake $\not\!\!E_T$ background events in the final selected sample.

Another source of background can happen when a lepton or a track within a jet is reconstructed as an isolated lepton or track. In the ee and $e\mu$ analyses, the amount of misidentified electron background is fitted to the observed distribution of electron likelihood in the data. We first determine the shape of the electron likelihood for real electrons in a pure $Z \to ee$ sample. The shape of the electron likelihood for the misidentified electron background is determined using a sample containing one 'probe' fake electron without the likelihood selection, and another electron candidate that satisfies an electron veto of $\chi^2_{hmx} > 50$ and $\mathcal{L} < 0.2$. Kinematic cuts require the event to be outside the $60 < M_Z < 130$ GeV mass window and have $\not\!\!E_T < 15$ GeV to reject Z and W boson events. This sample is dominated by misidentified electrons. The likelihood distribution of the probe fake electron is used for the misidentified electron template.

We measure the fraction f_μ of muons that appear as isolated in a di-muon control sample dominated by fake isolated muons. To suppress physics processes with real isolated muons the leading p_T muon is required to fail the muon criteria. This rejects both $Z \to \mu\mu$ events, and $W \to \mu\nu$ events where a second high p_T muon might arise from a muon in a jet. In the $\mu\mu$ channel, the number of events with a fake isolated muon contributing to the final sample is estimated using two linear equations from two samples: a 'tight' sample requiring two isolated muons, where isolated muon is defined by the relation $(d\mathcal{R}(\mu, jet) < 0.5)$; a 'loose' sample requiring only one isolated muon. In the $e\mu$ channel the contribution from events where both leptons are fake leptons is already accounted for when computing the misidentifed electron background. The remaining contribution (from events with a real electron and a fake isolated muon) is computed from the number of events in a sample where the electron and the muon have the same sign and where there is no muon isolation requirement, times the previously measured fraction f_μ.

Background yields for the ℓ+track channels are estimated using the following procedure. First, the selected events are split into four observed samples: N_{LL}, N_{LT}, N_{TL} and N_{TT} where the first subscript denotes the lepton and the second denotes the track. L or T refer to loose or tight leptons or tracks, respectively. These designations differ by the use or omission of the isolation criteria. These event counts are related to the number of events with actual real or fake leptons by the following system of equations:

$$\begin{aligned}
N_{LL} &= N_{rr} + N_{rf} + N_{fr} + N_{ff} \\
N_{LT} &= \epsilon^r_{track} N_{rr} + \epsilon^f_{track} N_{rf} + \epsilon^r_{track} N_{fr} + \epsilon^f_{track} N_{ff} \\
N_{TL} &= \epsilon^r_{lepton} N_{rf} + \epsilon^r_{lepton} N_{rf} + \epsilon^f_{lepton} N_{fr} + \epsilon^f_{lepton} N_{ff} \\
N_{TT} &= \epsilon^r_{lepton} \epsilon^r_{track} N_{rr} + \\
&\quad \epsilon^r_{lepton} \epsilon^f_{track} N_{rf} + \epsilon^f_{lepton} \epsilon^r_{track} N_{fr} + \epsilon^f_{lepton} \epsilon^f_{track} N_{ff}
\end{aligned} \tag{2}$$

where the first and second subscripts on the right side indicate the origin of the lepton and track, respectively. r indicates real leptons or tracks, and f indicates an instrumental origin for leptons or tracks. ϵ^r_{lepton} and ϵ^r_{track} are the efficiencies for the real lepton and track to pass the isolation requirement, and ϵ^f_{lepton},ϵ^f_{track} are the probabilities for the fake lepton and track to pass the isolation requirements. The total event yield from mismeasured processes is estimated as $N_{TT} - N_{rr}\epsilon^r_{lepton}\epsilon^r_{track}$.

For generating fake event samples, we use same sign dilepton events and remove the muon isolation/electron likelihood cuts and topological requirements.

The jet flavor composition of backgrounds is estimated with ALPGEN.

C. Composition of Observed Samples

The expected numbers of background and signal events in all five channels (assuming a top quark production cross section of 7 pb) are listed in Table I along with the observed number of candidates. More detailed breakdowns of events at different stages of the event selection are given in Table II and Table III for the e+track and μ+track channels, respectively.

Sample	$t\bar{t}$	WW	Z	Mis-id	Total	Data
$e\mu$	36.7 ± 2.4	1.7 ± 0.7	4.5 ± 0.7	2.6 ± 0.6	44.5 ± 2.7	39
ee	11.5 ± 1.4	0.5 ± 0.2	2.3 ± 0.4	0.6 ± 0.2	14.8 ± 1.5	17
$\mu\mu$	8.3 ± 0.5	0.7 ± 0.1	4.5 ± 0.4	0.2 ± 0.2	13.7 ± 0.7	13
$e + track$	9.4 ± 0.1	0.1 ± 0.0	0.4 ± 0.1	0.4 ± 0.1	10.3 ± 0.2	8
$\mu + track$	4.6 ± 0.1	0.1 ± 0.0	0.7 ± 0.1	0.1 ± 0.0	5.5 ± 0.1	6

TABLE I: Expected event yields for signal and various backgrounds and number of observed events for the five channels.

TABLE II: Expected and observed e+track event yields from background and signal $\sigma_{t\bar{t}} = 7.0$ pb processes.

cut	$t\bar{t} \to e + track$	WW	$Z \to ee$	$Z \to \tau\tau$	Mis-id	total	observed
dilepton vetoes	20.0 ± 0.1	9.0 ± 0.2	619.8 ± 10.3	20.0 ± 1.9	42.1 ± 2.9	710.9 ± 11.1	712
2 jets	15.9 ± 0.1	4.5 ± 2.6	145.4 ± 4.0	4.1 ± 0.5	24.1 ± 2.6	194.1 ± 4.9	185
$\not\!\!E_T$and $\not\!\!E_T{}^{Z_{fit}}$	13.6 ± 0.1	1.0 ± 2.3	4.4 ± 0.4	2.4 ± 0.4	13.4 ± 2.3	34.7 ± 2.3	28
MEDIUM b tag	9.4 ± 0.1	0.1 ± 0.0	0.3 ± 0.0	0.1 ± 0.0	0.5 ± 0.1	10.4 ± 0.1	8

TABLE III: Expected and observed μ+track event yields from background and signal $\sigma_{t\bar{t}} = 7.0$ pb processes.

cut	$t\bar{t} \to \mu + track$	WW	$Z \to \mu\mu$	$Z \to \tau\tau$	Mis-id	total	observed
dilepton vetoes	10.5 ± 0.1	8.1 ± 0.2	610.2 ± 8.2	7.1 ± 0.7	1.2 ± 0.5	637.0 ± 8.2	645
2 jets	8.2 ± 0.1	4.4 ± 0.1	183.9 ± 3.3	3.0 ± 0.4	0.8 ± 0.2	200.2 ± 3.3	207
$\not\!\!E_T$and $\not\!\!E_T{}^{Z_{fit}}$	6.8 ± 0.1	0.7 ± 0.1	12.6 ± 0.2	1.6 ± 0.3	0.4 ± 0.1	22.0 ± 0.4	29
MEDIUM b tag	4.6 ± 0.1	0.1 ± 0.0	0.6 ± 0.1	0.1 ± 0.0	0.1 ± 0.0	5.4 ± 0.1	6

Comparison plots between data and the signal+background simulations provide a check of the kinematic properties of our data sample with expected signal and background distributions. Figure 1 shows the comparison of $\not\!\!E_T$ in data and simulation for the ee channel in the $Z \to ee$ enriched sample. Figure 1 also shows the comparison of DATA and simulation for the invariant mass of the lepton and isolated track for the ℓ+track channel in the Z boson enriched sample. The invariant mass peaks approximately at 90 GeV as expected. Figures 2 and 3 indicate the $\not\!\!E_T$ distributon in the ℓ+track sample before and after $b-$tagging is applied, respectively. To within the statistics available, no discrepancies are observed.

V. KINEMATIC RECONSTRUCTION

Use of the kinematic measurements in events from $t\bar{t}$ production and constraints available from the $t\bar{t}$ assumption allows a partial reconstruction and a determination of m_t. Given the decay chain of each top quark to a W boson and a b quark, and each W boson to a charged lepton plus a neutrino, there are six final state particles: two charged

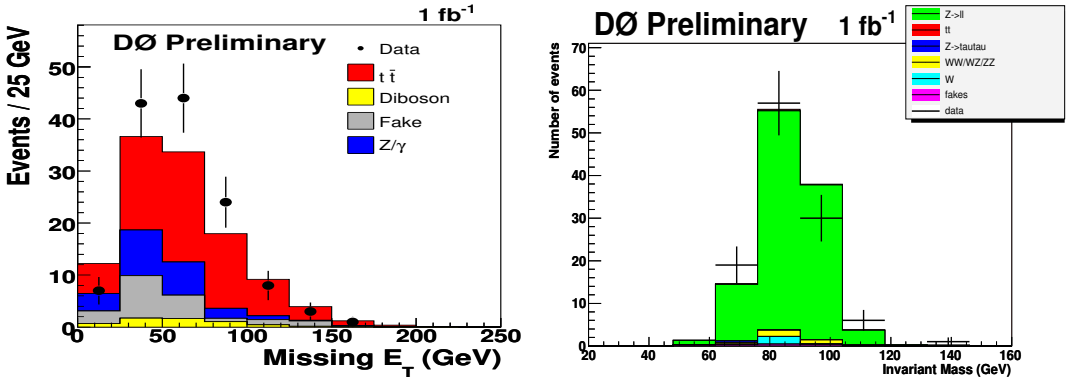

FIG. 1: DATA/MC comparison for the combination of dilepton channels (left) for $\not\!\!E_T$ and for the ℓ+track (right) channel for invariant mass of the lepton and track and in the Z background enriched sample.

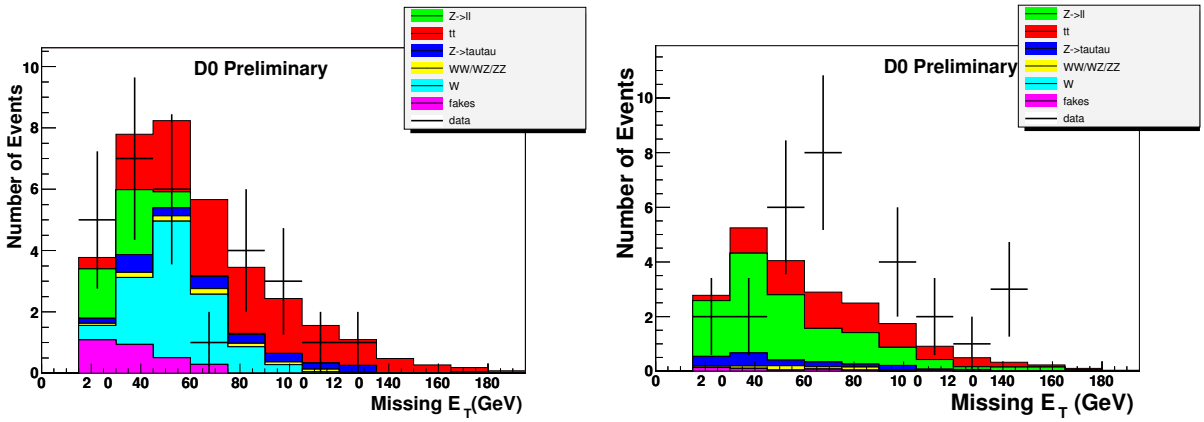

FIG. 2: $\not\!\!E_T$ for signal and background processes overlaid with observed data events for the $e+track$ (left) and $\mu+track$ (right) channels. Events have at least 2 jets and no $b-$tagging is applied.

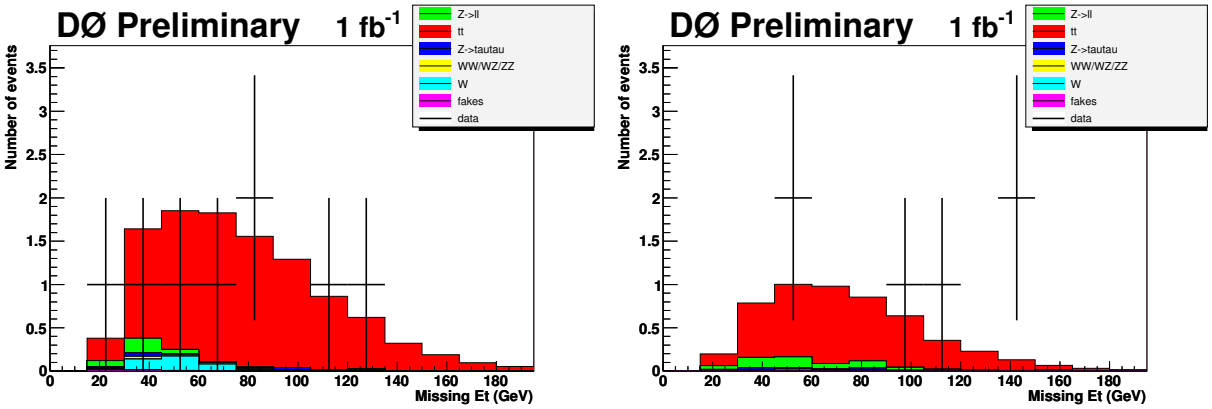

FIG. 3: $\not\!\!E_T$ for signal and background processes overlaid with observed data events for the $e+track$ (left) and $\mu+track$ (right) channels. Events have at least 2 jets, one of which is $b-$tagged.

leptons, two neutrinos, and two $b-$quarks. Each particle, i, may be described by three momentum components. Of these 18 independent parameters, we may directly measure the full momenta for the leptons. The leading two jets tend strongly to be from the $b-$quarks. Despite final state radiation and fragmentation, the jet momenta are strongly correlated with those of the underlying $b-$quarks. We also have two cumulative components ($\not\!\!E_x$ and $\not\!\!E_y$) from the neutrinos. These leave four parameters unknown. Two further constraints are supplied by relating the four-momenta

of these particles to masses of each of the W bosons in the decay:

$$\begin{aligned} M_{W_1}^2 &= (E_{\nu_1} + E_{l_1})^2 - (\vec{p}_{\nu_1} + \vec{p}_{l_1})^2 \\ M_{W_2}^2 &= (E_{\nu_2} + E_{l_2})^2 - (\vec{p}_{\nu_2} + \vec{p}_{l_2})^2 \end{aligned} \tag{3}$$

where subscript 1 indicates the $\ell\nu$ pair coming from one W boson, and subscript 2 indicates the $\ell\nu$ pair coming from the other W boson. Another constraint is supplied by requiring that the mass of the top quark and the mass of the anti-top quark be equal.

$$(E_{\nu_1} + E_{l_1} + E_{b_1})^2 - (\vec{p}_{\nu_1} + \vec{p}_{l_1} + \vec{p}_{b_1})^2 = (E_{\nu_2} + E_{l_2} + E_{b_2})^2 - (\vec{p}_{\nu_2} + \vec{p}_{l_2} + \vec{p}_{b_2})^2 \tag{4}$$

Without supplying further information, we have an underconstrained $-1C$ fit. Some other information must be supplied to solve these equations.

A. Neutrino Weighting

In the neutrino-weighting approach [11], the top quark mass is supplied as an input parameter to permit solutions to Equations 3 and 4. To determine which values of m_t are more consistent with an event's measured kinematics, we omit the $\not\!\!E_T$ measurements in favor of sampling from expected distributions of neutrino rapidity for each of the two top quarks. The distribution of neutrino rapidities was extracted from several simulated $t\bar{t}$ samples with different values of m_t at generator level. These distributions are described by a single Gaussian with a standard deviation that is weakly dependent on the top quark mass. Variations between channels arise from different selection criteria.

This procedure results in a net addition of one constraint. This makes the problem solvable to obtain the momentum of each of the two neutrinos. We try each of two assumptions pairing the leading two jets with the W bosons identified by the charged leptons. The constraint equations are quadratic for each neutrino, so one can have 0, 1, 2 or 4 real solution combinations for each jet-lepton configuration.

For each pairing of neutrino solutions, the expected $\not\!\!E_T$ can be calculated from the neutrino momenta required by the solution. This is compared to the measured $\not\!\!E_T$ in the event by allowing for an independent Gaussian resolution in $\not\!\!E_x$ and $\not\!\!E_y$. A weight, ω, is calculated as:

$$\omega = \frac{1}{N_{\text{iter}}} \sum_{i=1}^{N_{\text{iter}}} \exp\left(\frac{-(\not\!\!E_{x,i}^{\text{calc}} - \not\!\!E_x^{\text{obs}})^2}{2\sigma^2_{\not\!\!E_x^{unc}}}\right) \exp\left(\frac{-(\not\!\!E_{y,i}^{\text{calc}} - \not\!\!E_y^{\text{obs}})^2}{2\sigma^2_{\not\!\!E_y^{unc}}}\right) \tag{5}$$

where $\not\!\!E_T^{obs}$ is the measured event $\not\!\!E_T$ and $\not\!\!E_T^{calc}$ is the $\not\!\!E_T$ calculated from the p_x^ν's and p_y^ν's resulting from each solution. The sum is taken over N_{iter} which includes solutions for all neutrino η assumptions and all jet-lepton assignment combinations. Since the reconstructed high p_T objects enter into both $\not\!\!E_T^{calc}$ and $\not\!\!E_T^{obs}$, the unclustered E_T is the element which should connect them if the $t\bar{t}$ hypothesis is correct. Hence $\sigma_{\not\!\!E_x^{unc}}$ and $\sigma_{\not\!\!E_y^{unc}}$ stand for the resolution of $\not\!\!E_x$ and $\not\!\!E_y$ attributable to unclustered energy fluctuations.

The parameter ω reflects the agreement between the measured and calculated $\not\!\!E_T$. The resolution $\sigma_{\not\!\!E_{x,y}}$ is a parameter of the method and affects the sensitivity to the top quark mass. It has been studied in $Z \to ee + 2$ jet collider data and Monte Carlo events. The unclustered $\not\!\!E_T$ components are calculated as

$$\not\!\!E_{x,y}^{unc} = \not\!\!E_{x,y} + \sum_{jets} p_{x,y} + \sum_{electrons} p_{x,y} \tag{6}$$

In both data and simulation, the resolution of these components is studied as a function of the unclustered scalar E_T,

$$S_T^{unc} = \sum_{cells} E_T - \sum_{jets} p_T - \sum_{electrons} p_T \tag{7}$$

As shown in Figure 4, the dependence for Monte Carlo can be expressed in the following form:

$$\sigma_{\not\!\!E_x^{unc}}(S_T^{unc}) = \sigma_{\not\!\!E_y^{unc}}(S_T^{unc}) = 4.38 + 0.52\sqrt{S_T^{unc}} \tag{8}$$

Because of the good agreement between data and Monte Carlo the parametrization obtained for Monte Carlo was used as an unclustered missing energy resolution for both data and Monte Carlo in Eqn. (5).

For each event, we consider ten different rapidity assumptions for each of the two neutrinos in each event. We step through Gaussian histograms that have the standard deviation appropriate to a given top quark mass. The choice of η is made so that the same number of top quark events is expected for each of the η ranges; that is, each η value represents 10% of the top sample. We choose those η values which are the medians in each of the ten bins.

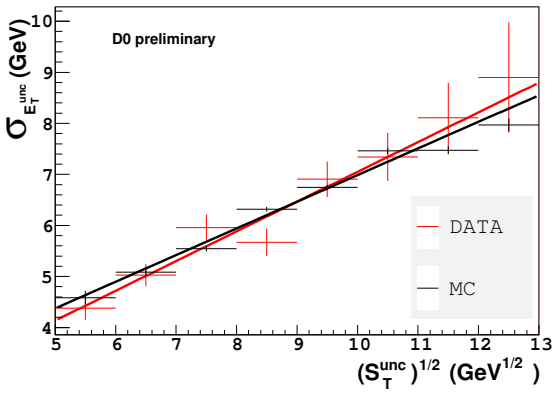

FIG. 4: Dependence of resolution of unclustered missing energy on unclustered scalar transverse missing energy for $Z \rightarrow ee$ sample with exactly 2 jets.

The actual η values taken are defined such that they divide these samples into two equal parts. We sum the weights for all configurations to obtain a total weight for a given top mass. This process is repeated for a range of assumed top masses from 80 GeV through 330 GeV.

The weight curve calculation for a given event accounts for the detector resolution of the $\not\!\!E_T$ measurement, but jet and lepton energies may also be mismeasured. As a result, some configurations which are consistent with a top quark mass hypothesis are either not solvable at reconstruction level or produce a weight that is incorrectly estimated. Detector resolutions are accommodated in the weight curve calculation in the following manner: for each configuration of each event, 150 cases are calculated in which all jets and leptons are independently fluctuated according to their known resolutions. This way, 150 different samples of the event weight around the nominal jet and lepton measurements are obtained and summed. The effect can be seen for some example signal events in Figure 5. The weight curves become smoother and the range of top quark mass solutions increases. The number 150 was found to be sufficient to obtain stable and smooth weight curves as well as to have acceptable computation times. The rate to get solutions for $t\bar{t}$ $e\mu$ events is 95.9% with no smearings and 99.5% with 150 smearings. For data events, the number of smears is also set at 150.

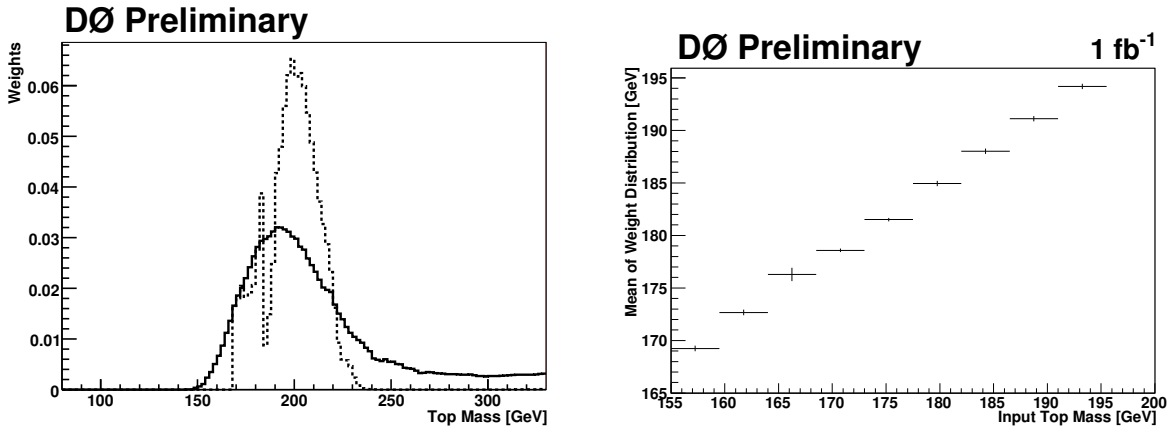

FIG. 5: Normalized weight distribution (left) for an example simulated signal event with $m_t = 175$ GeV. The dashed distribution has no detector smearing, while the solid distribution has been smeared 150 times. At right is the correlation between the mean of the weight distribution and the input m_t.

We normalize the total event weight distribution to unity for each event so that each event is treated equally within a data sample. Weight distributions from individual events have fluctuations due largely to the partially reconstructed nature of the events. Various properties of these weight distributions, however, are strongly correlated with the actual top quark mass. For instance, the right of Fig. 5 illustrates the strong correlation of the mean of the weight distribution on the input top quark mass from the Monte Carlo. We describe optimal use of the weight

distribution's information to extract an m_t measurement in the next section.

VI. EXTRACTING THE TOP QUARK MASS

The kinematic reconstruction provides an estimate of the most probable mass range consistent with the kinematics of each candidate event. It remains to extract a calibrated m_t measurement from an experiment with several signal and background events. Previous analyses have either relied on the most probable mass from the weight distribution, m_{pk}, such as CDF's νWT measurement [13] and DØ's MWT measurement [12] in Run II. Other measurements relied on several parameters taken as the coarsely binned weight distribution itself, such as the DØ mass measurements in Run I [11] or the νWT measurement in Run II [12]. The coarse template approaches generally extract better statistical performance than single parameter methods by using more information, but at the cost of computational resources and complexity. We have attempted to address these issues directly for the νWT analysis described below.

A. Multiple Parameter Fitting and Optimization

The question arises whether further information is available to further improve the statistical uncertainty from a single parameter fit. Earlier efforts have indicated that up to a 20% improvement in uncertainty was possible with a binned template. So the next step is to define the optimal set of input variables for the top quark mass extraction. When selecting such input variables, we sought to minimize the statistical uncertainty while also keeping the computational complexity of the analysis low.

We begin generally by designating a set of input variables characterizing the weight distribution by $\{x_i\}_N$, where N is the number of variables. Examples of $\{x_i\}_N$ might be the integrated weight in bins of a coarsely binned template, or they might be the list of moments of the weight distribution. A Probability Density Histogram (PDH) for simulated signal events, h_s, is defined as an $(N+1)-$dimensional histogram of input top quark mass vs. N variables. The PDH for the background, h_b, is defined as an $N-$dimensional histogram of the $\{x_i\}_N$. Both h_s and h_b are normalized, so that:

$$\int_\Omega h_s(x_{iN}, m_t)\, d\{x_i\}_N \;=\; 1 \tag{9}$$

$$\int_\Omega h_b(x_{iN})\, d\{x_i\}_N \;=\; 1 \tag{10}$$

After having modeled $h_s(x_{iN}, m_t)$ and $h_b(\{x_i\}_N)$, m_t is extracted using a maximum likelihood method. For each event in a given ensemble, all $\{x_i\}$ are found and used for the likelihood calculation. The likelihood $\mathcal{L}$ is given by:

$$\mathcal{L}(\{x_i\}_N, \bar{n}_b, N_{obs} \mid m_t) \;=\; \prod_{i=1}^{N_{obs}} \frac{n_s h_s(x_{iN} \mid m_t) + n_b h_b(x_i)}{n_s + \bar{n}_b}. \tag{11}$$

where N_{obs} is the number of events in the sample and $n_s = N_{obs} - \bar{n}_b$. The result is a histogram of likelihood vs. m_t for the ensemble. In order to extract the most likely top quark mass and error, we perform a parabolic fit to the $-\log\mathcal{L}$.

Measurements of m_t for several channels are obtained by multiplying the likelihoods of each channel. This is equivalent to adding up the negative log likelihoods of every channel:

$$-\log\mathcal{L} = \sum_{ch}(-\log\mathcal{L}_{ch}) \;\;, \tag{12}$$

where ch denotes the dilepton channel: $ch \in \{e\mu, ee, \mu\mu\}$, the ℓ+track channel: $ch \in \{e+track, \mu+track\}$ or the full combination: $ch \in \{e\mu, ee, \mu\mu, e+track, \mu+track\}$, respectively.

We have performed the analysis with many different choices of variables from the weight distributions. These included single parameter choices such as the most probable mass, m_{pk}, and the mean, μ_w, of the distribution. These two variables provide similar performance in the range 140 GeV $< m_t <$ 200 GeV. Vectors of multiple parameters included various coarsely binned templates, or subsets of their bins. We also investigated the use of the moments of the weight distribution. This was motivated partly by the observation that event-by-event fluctuations were reduced by looking at bulk properties of the weight distribution. The most efficient use of the information came from using the first two moments (μ_w and root-mean-squared, σ_w) of the weight distribution. This gave 16% better expected statistical uncertainty than just using m_{pk} or μ_w alone. No other choice of variables gave significantly better performance.

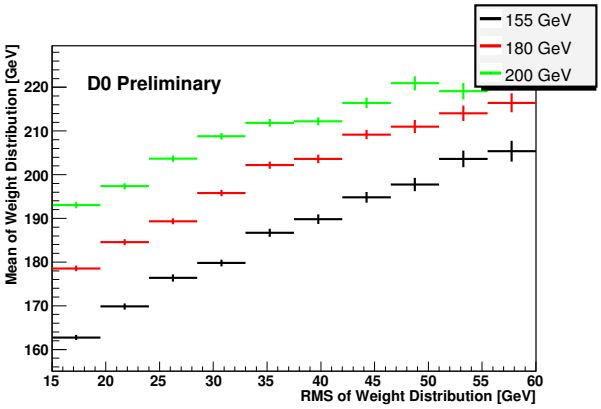

FIG. 6: The correlation between the Root Mean Square of the weight distribution and mean for the $e\mu$ channel. Three test masses of 155 GeV, 180 GeV and 200 GeV are shown.

The choice of first two moments works in the following way. The σ_w is strongly correlated with μ_w for a given input top quark mass. This is shown in Figure 6 for three different input top quark masses. The value of σ_w helps to better identify the range of input m_t that are most consistent with the given event having result μ_w. This ability to de-weight incorrect m_t assignments results in a narrower likelihood distribution and causes a corresponding reduction in the statistical uncertainty.

B. Probability Density Functions

Due to limited statistics in some simulated samples there are fluctuations in h_s and h_b that should be smoothed. For this reason, we have performed fits to these PDH's to extract a measurement. For the signal, we generate a Probability Density Function (PDF) by fitting h_s with the functional form:

$$\begin{aligned} f_s(\mu_w,\sigma_w,m_t) &= p_6\cdot(\sigma_w+p_{14})^{p_7}\exp(-p_8(\sigma_w+p_{14})^{p_9}) \\ &\times\Bigg[(1-p_{10})\frac{1}{\sigma\sqrt{2\pi}}\exp(-\frac{(\mu_w-m)^2}{2\sigma^2}) \\ &+p_{10}\cdot\frac{p_{12}^{1+p_{13}}}{\Gamma(1+p_{13})}(\mu_w-\frac{m}{p_{11}})^{p_{13}}\exp(-p_{12}(\mu_w-\frac{m}{p_{11}})) \\ &\times\Theta(\mu_w-\frac{m}{p_{11}})\Bigg] \\ &\times\left[\int_0^\infty p_6\cdot(\mathrm{x}+\mathrm{p}_{14})^{\mathrm{p}_7}\exp(-\mathrm{p}_8(\mathrm{x}+\mathrm{p}_{14})^{\mathrm{p}_9})\mathrm{dx}\right]^{-1} \end{aligned} \tag{13}$$

where the integral is for normalization. The parameters m and σ represent linear transformations of μ_w and σ_w, respectively,

$$\begin{aligned} m &:= p_0+p_1(\sigma_w-36\text{ GeV})+p_2(m_t-170\text{ GeV}) \\ \sigma &:= p_3+p_4(\sigma_w-36\text{ GeV})+p_5(m_t-170\text{ GeV}). \end{aligned} \tag{14}$$

An example of a two-dimensional slice of a three-dimensional fit for the input top quark mass of 170 GeV is shown in Figure 7.

The background probability density function $f_b(\mu_w,\sigma_w)$ is obtained as the normalized two-dimensional function of μ_w and σ_w of simulated background events:

$$f_b(\mu_w,\sigma_w) = \frac{\exp\left(-(p_4\mu_w+p_5\sigma_w-p_0)^2/(2p_1^2)-(p_6\mu_w+p_7\sigma_w-p_2)^2/(2p_3^2)\right)}{\int_0^\infty\int_0^\infty\exp\left(-(p_4\mathrm{x}+\mathrm{p}_5\mathrm{y}-\mathrm{p}_0)^2/(2\mathrm{p}_1^2)-(\mathrm{p}_6\mathrm{x}+\mathrm{p}_7\mathrm{y}-\mathrm{p}_2)^2/(2\mathrm{p}_3^2)\right)dx\,dy} \tag{15}$$

We motivate this fit function in the following way. There is a linear relationship between rms and mean as it is seen from Fig. 7. We want to have a fit function which can describe the slice of the μ_w distribution for a given σ_w

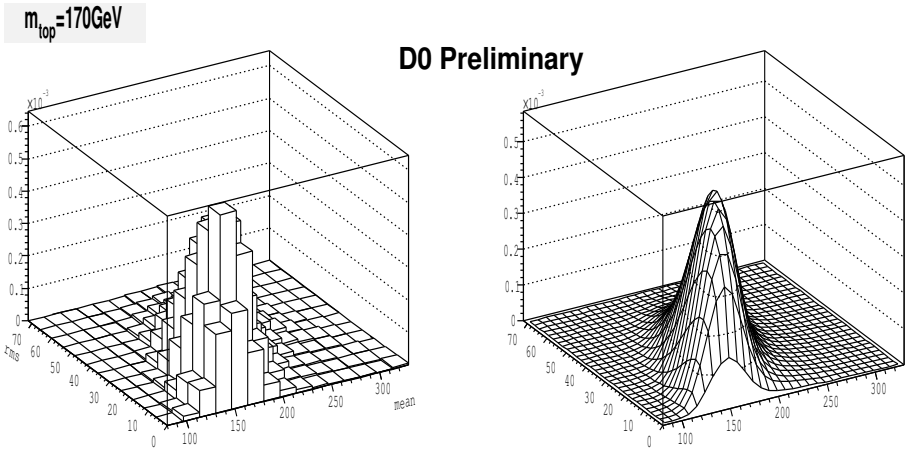

FIG. 7: The histogram μ_w vs. σ_w at a constant m_t is shown (left). The corresponding view of the 3d-fit result is at right. Results for $e\mu$ channel with $m_t = 170$ GeV.

(and a given m_t). It is best if this fit function is of the same form for each value of the σ_w, a gaussian convoluted with polynomial and falling exponential (Eq. 13). Since the σ_w varies with μ_w, we need the center of the gaussian to shift as the σ_w (and m_t) changes. Eq. 14 accounts for this effect.

After having modeled f_s and f_b, m_t is extracted using a maximum likelihood method. To measure the top quark mass more accurately, the following procedure was employed. Two extra terms were added to the likelihood $\mathcal{L}$. The first term is a constraint that requires that the fitted sum of the number of signal events n_s and number of background events n_b agrees within Poisson fluctuations with the number of observed events, N_{obs}:

$$\mathcal{L}_{\rm poisson}(n_s + n_b, N_{obs}) \equiv \frac{(n_s + n_b)^{N_{obs}} e^{-(n_s+n_b)}}{N_{obs}!}. \tag{16}$$

The second part is a Gaussian constraint that requires agreement between the fitted number of background events n_b and the number of expected background events $\bar{n}_b$ within Gaussian fluctuations, where the width of the Gaussian is given by the estimated uncertainty δ_b on $\bar{n}_b$:

$$\mathcal{L}_{\rm gaus}(n_b, \bar{n}_b, \delta_b) \equiv \frac{1}{\sqrt{2\pi}\delta_b} e^{[-(n_b-\bar{n}_b)^2/2\delta_b^2]}. \tag{17}$$

The total likelihood is given by:

$$\mathcal{L}(\mu_{wi}, \sigma_{wi}, \bar{n}_b, N_{obs} \mid m_t, n_s, n_b) = \tag{18}$$

$$\mathcal{L}_{\rm gaus}(n_b, \bar{n}_b, \delta_b)\mathcal{L}_{\rm poisson}(n_s + n_b, N_{obs}) \prod_{i=1}^{N_{obs}} \frac{n_s f_s(\mu_{wi}, \sigma_{wi} \mid m_t) + n_b f_b(\mu_{wi}, \sigma_{wi})}{n_s + n_b}. \tag{19}$$

As in the PDH approach, the product extends over all events in the data ensemble.

The maximum of the likelihood corresponds to the measured top quark mass. Since $-\log\mathcal{L}$ is given by an analytic expression, it can be minimized simultaneously with respect to m_t, n_s, and n_b. This is done via MINUIT [23, 24]. The result of this minimization is our top quark mass estimate, $\hat{m}_t$. Its statistical uncertainty $\hat{\sigma}_{m_t}$ is found by fixing the n_s, and n_b to their optimal values and taking half of distance between the points at which the $-\log\mathcal{L}$ value is 0.5 units greater than its minimum value.

Measurements of m_t for several channels are obtained by minimizing the combined $-\log\mathcal{L}$ simultaneously with respect to m_t and number of signal and background events for the channels considered.

C. Ensemble Testing and Performance

The performance and precision of the method is tested in pseudo-experiments, or 'ensemble' tests. An ensemble is a set of simulated events of the same size as the selected dataset. The composition of signal and background events corresponds to the expected composition in data. Ensembles are created by randomly drawing simulated events out

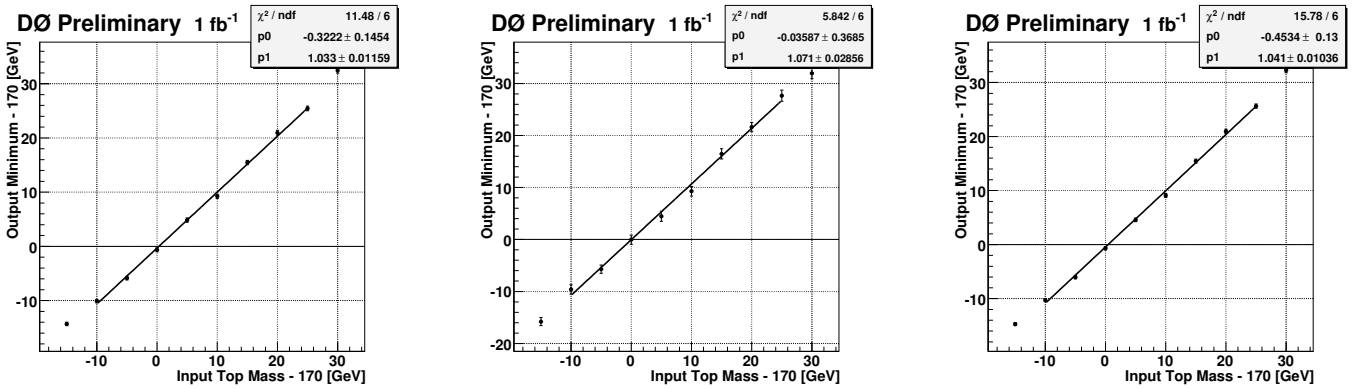

FIG. 8: The combined calibration curves corresponding to the PDF method. Top quark mass estimate for the dilepton channels (left top) $lepton + track$ channels (middle) and all channels (right). Overlaid is the result of the linear fit as defined in Eqn. 20.

Channel	Slope: α	Offset: β [GeV]	Pull Width	Expected Statistical Uncertainty, GeV
dilepton (PDF)	1.03 ± 0.01	-0.32 ± 0.15	1.06 ± 0.02	5.77
ℓ+track (PDF)	1.07 ± 0.03	-0.04 ± 0.37	1.07 ± 0.02	12.88
combined (PDF)	1.04 ± 0.01	-0.45 ± 0.13	1.06 ± 0.02	5.28

TABLE IV: Slope and Offset from the linear fit in Eqn. 20 to the calibration curve in Fig. 8 for the five different channels with the PDF method.

of a large ensemble pool. The number of background events of each source is Poisson fluctuated around the expected yields. The remaining events in the ensemble are signal events. This way there is no explicit use of the $t\bar{t}$ production cross section, which is a function of the top quark mass. A calibration curve for the top quark mass estimator can be obtained, because the true top quark mass is known for ensembles. The generated input top quark mass $m_t^{\rm gen}$ is parametrized as a function of the output top quark mass $\hat{m}_t$.

The performance of the method is evaluated by extracting the top quark mass in 300 pseudo-experiments. Each pseudo-experiment is a mass measurement performed on ensembles with the number of simulated events set to the number observed in each of the five channels, as itemized in Table I. The size of the ensemble reflects the number of selected events in the respective datasets. The events in a pseudo-experiment for a generated top quark mass $m_t^{\rm MC}$ are randomly chosen from the corresponding signal and background Monte Carlo sample. For a given background process, the number of events in an ensemble is Poisson-distributed around the expected yield. This approach guarantees that the mass measurement is not biased by the cross section for top quark production, which is mass-dependent.

Averaging the measurements of all 300 ensembles for a given generated input top quark mass $m_t^{\rm input} \equiv m_t^{\rm MC}$, one obtains a calibration curve which shows the measured output top quark mass $m_t^{\rm output} \equiv \hat{m}_t$ as a function of the generated input top quark mass. The calibration curves for the dilepton and ℓ+track channels are obtained by summing all negative logarithms of likelihoods for each test mass. They are shown in Fig. 8. In each channel a linear fit is performed giving:

$$m_t^{\rm output} = \alpha \cdot (m_t^{\rm input} - 170\ {\rm GeV}) + \beta\ {\rm GeV} + 170\ {\rm GeV} \tag{20}$$

The results of the fits are summarized in Tab. IV. Ideally, $\alpha = 1$ and $\beta = 0$. The mean value of the data measurement is corrected for the slope and offset of these calibration curves.

The pull is defined as:

$$\text{pull} = \frac{\rm m_t - m_t^{gen}}{\sigma(\rm m_t)}, \tag{21}$$

where $m_t \pm \sigma(m_t)$ is the measured top quark mass and uncertainty after the calibration. The ideal pull distribution has a Gaussian shape with the mean at zero and a width of one. The pull widths from ensemble tests are given in Table IV. A pull width larger (less) than one indicates an underestimated (overestimated) statistical uncertainty.

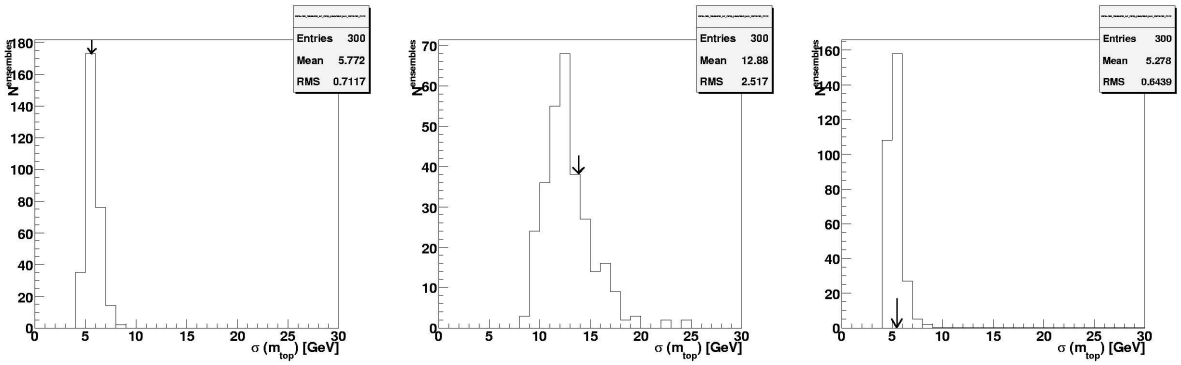

FIG. 9: Distribution of statistical uncertainties for top mass measurements of 300 pseudo experiments for the 2ℓ (left), ℓ+track (middle) and all channels (right) for simulated events with $m_t = 170$ GeV for the PDF method. The uncertainties are corrected by the calibration curve and for the pull width. The arrows mark the observed uncertainty in data.

The uncertainty of the data measurement is corrected for deviations of the pull width from one as well as the slope of the calibration curve. The mean of the distribution of calibrated and pull-corrected statistical uncertainties yields the expected statistical uncertainty (see Table IV). The pull corrected statistical uncertainty equals the statistical uncertainty multiplied by the respective pull width. Figure 9 shows the pull width corrected distribution of statistical uncertainties for top mass measurements from the ensemble testing. The expected uncertainty on the combined measurement for all channels is 5.3 GeV for the PDF method.

VII. RESULTS

Employing the PDF method and Eq. 19, we obtained a calibrated mass and statistical uncertainty for the two channels and combined measurement:

$$\begin{aligned} \text{dilepton} : \mathrm{m_t} &= 176.1 \pm 5.8\ (\text{stat.})\ \text{GeV} \\ ee + \mu\mu only : m_t &= 182.6 \pm 8.5\ (\text{stat.})\ \text{GeV} \\ \ell + \text{track} : \mathrm{m_t} &= 174.6 \pm 12.8\ (\text{stat.})\ \text{GeV} \\ \text{combination} : \mathrm{m_t} &= 176.0 \pm 5.3\ (\text{stat.})\ \text{GeV} \end{aligned}$$

The projection of the 3-dimensional $-\log\mathcal{L}$ fit as a function of top quark mass for the dilepton, ℓ+track, and the combination of all channels before the calibration are shown in Figure 10. As a cross-check, we applied the the PDH approach and Eq. 11 and obtained a similar mean value for m_t.

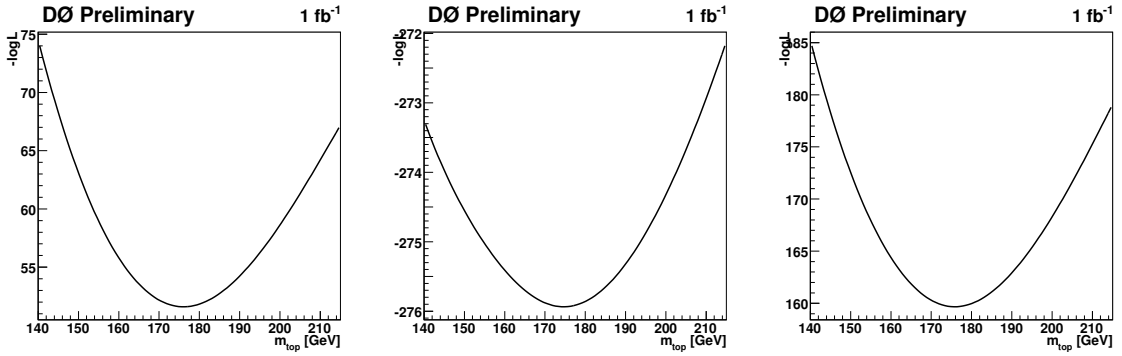

FIG. 10: Negative log likelihood distributions for the 2ℓ, ℓ+track and the combination of all channels respectively before calibration. PDF method shown.

A. Systematic Uncertainties

The top quark mass measurement relies substantially on the Monte Carlo simulation of $t\bar{t}$ signal and backgrounds. While we have made systematic adjustments to this model to account for the performance of the detector, residual uncertainties remain which can manifest as systematic shifts to the measured mass. The modeling of physics may also cause such shifts. There are four primary categories of systematic uncertainty: calibration of jet energies, modeling of the physics of jets, jet and lepton resolutions and efficiencies, and the modeling of background and signal event rates and kinematic shapes. We have estimated each of these as follows.

a. **Jet Energy Calibration Uncertainty:** Because the $b-$jets encompass the largest share of the energy in top quark events, their calibration has the largest implication for the uncertainty in m_t. Ideally, the procedure to calibrate jet energies in data and Monte Carlo will achieve the same energy scale in both. However, a small uncertainty in any residual mismatch remains. We estimate this by repeating the ensemble testing with simulated events where the jet energies are shifted up and down by the known p_T dependent uncertainty. The probability density histograms (h_s, h_b) and functions (f_s, f_b) are left with the nominal calibration. Fig. 11 shows the calibration curve before and after the shift of the jet energy scale. The uncertainty is found to be $\pm$ 1.6 GeV.

A second component to the jet energy calibration arises because the jets in signal events are primarily $b-$jets. These have different detector response than the light quark and gluon jets which dominate the sample used to derive the overall calibration. By applying this calibration to the $b-$jet sample, a 1.8% shift in jet p_T is observed [25]. We adjust jets for this and propagate the correction into the $\not\!\!E_T$. This causes a shift of 0.4 GeV in the measured m_t which is taken as an uncertainty.

After the initial calibration, a residual shift in jet p_T distributions is observed in the $Z+$jets and $W+$jets samples when comparing data and Monte Carlo. We adopt a further calibration that improves agreement in these distributions, and apply it to all of our background samples. It is uncertain whether this adjustment is appropriate to $t\bar{t}$ signal events. Therefore, we take the impact on the measured m_t, determined to be 0.4 GeV in ensemble tests, to be a systematic uncertainty.

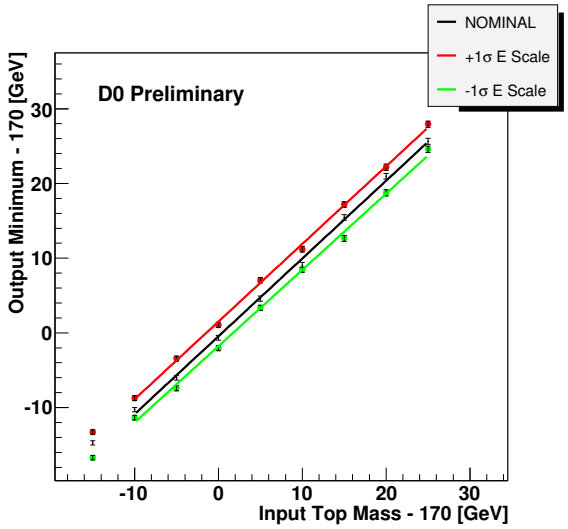

FIG. 11: Calibration curves after shifting the jet energy scale up and down by 1σ for the combination. *PDF* method shown.

b. **Jet Modeling Uncertainties:** An additional systematic uncertainty arises from the different models of b quark fragmentation. This systematic unceratinty was found by reweighting signal events with the b fragmentation processor in the Bowler scheme and then comparing the measured value to the nominal mass. It was found to be 0.5 GeV.

Extra jets in top quark events from gluon radiation can affect the $t\bar{t}$ p_T spectrum. This can impact the measured m_t. While our models describe the data within uncertainties for all channels, the ratio of 2 jet exclusive events to $\geq$ 3 jet events is typically 4 in the Monte Carlo and 3 in the data. To assess the impact of this difference, the simulated events for the top mass of 170 GeV are reweighted such that this ratio is the same. The ensemble tests with reweighted events are compared with nominal ensemble tests and the systematic uncertainty is found to be 0.1 GeV.

c. **Object Momentum Resolution and Efficiency Uncertainties:** To improve the agreement of data and Monte Carlo jet resolutions, an additional smearing is applied to signal Monte Carlo events. The ensemble testing is repeated by adjusting this smearing up and down within its uncertainty while keeping the probability density histograms and functions with the nominal resolutions. The effect is found to give a 0.1 GeV shift in m_t. A systematic uncertainty arising from the μ and isolated track p_T resolutions was similarly estimated at 0.1 GeV.

Residual uncertainties in the efficiencies from triggering, luminosity profiles, lepton identification and $b-$tagging exist between data and Monte Carlo. In each case, a respective systematic uncertainty on m_t was found by reweighting events according to the differences in selection efficiencies. The cumulative uncertainty was found to be 0.3 GeV.

d. **Signal and Background Modeling:** The uncertainty from the background kinematic shape is conservatively found by substituting for ensemble testing all background samples with the WW samples. The uncertainty was taken as the difference between the average measured top quark mass with this assumption to the nominal value, 0.3 GeV.

To estimate the impact of our uncertainty on background event yield, we varied the total background yield by its known uncertainty up and down keeping the relative ratios of individual background processes constant. The background yield uncertainty is found to be 0.1 GeV

To account for variations in the accuracy of signal models, we have compared ensemble test results using $t\bar{t}$ generated with ALPGEN with those using purely PYTHIA. Samples with $m_t = 170$ GeV were used. The difference between the two estimated masses was corrected by subtracting the expected statistical uncertainty divided by the square root of number of ensembles. The corrected uncertainty was determined to be 0.8 GeV.

The uncertainty from the choice of parton distribution function is estimated by reweighting the Monte Carlo up and down according to 20 available errors for CTEQ6.1. For each choice a new mass was measured and the difference between the mass obtained with reweighting and a nominal mass was recorded. The resulting error is the sum in quadrature of all above errors, found to be 0.3 GeV.

Source	PDF Uncertainties (GeV)
Jet Energy Scale	1.6
b-Jet Energy Scale	0.4
Sample Dependent JES	0.4
b fragmentation	0.5
Jet Resolution	0.1
Muon/Track Resolution	0.1
Selection Efficiency	0.3
$t\bar{t}$ + jets	0.1
Signal Modelling	0.8
PDF variation	0.3
Background Template Shape	0.3
Background Yield	0.1
Total Systematic Error	2.0

TABLE V: Summary of systematic uncertainties for the combined analysis of five 2ℓ and ℓ+track channels. The PDF method results are shown.

A summary of estimated systematic errors for the combined dilepton and ℓ+track channels is provided in Table V. The total uncertainty is conservatively found by assuming all the contributions are independent and adding them in quadrature. The systematic uncertainties in the PDF method are 2.0, 2.5 and 2.0 GeV for the 2ℓ, ℓ+track and combined measurements, respectively.

VIII. CONCLUSIONS

In 1 fb^{-1} of proton-antiproton collision data, we have used the neutrino weighting method to extract a top quark mass estimate from $t\bar{t}$ events in the 2ℓ and ℓ+track final states. We have performed an analysis based on the outputs of a kinematic reconstruction using assumed neutrino rapidity inputs. Using the moments of the resulting weight distribution, we have fitted probability density functions which relate these moments to the pole m_t for signal events. Using these templates and analogous ones for background, we measure a combined result from five dilepton channels:

$$m_t \;=\; 176.0 \;\pm 5.3\ (\text{stat.})\,\text{GeV} \pm 2.0\ (\text{syst.})\,\text{GeV}. \tag{22}$$

A cross-check was performed using the underlying probability density histograms directly and gave similar results. Our result is consistent with the current world average value of m_t [26].

---

[1] DØ Collab. (S. Abachi et al.), *Phys. Rev. Lett.* **74**, 2632 (1995).
[2] CDF Collab. (F. Abe et al.), *Phys. Rev. Lett.* **74**, 2626 (1995).
[3] C. T. Hill, *Phys. Lett.* B **345**, 483 (1995).
[4] K. Lane and E. Eichten, *Phys. Lett.* B **352**, 382 (1995); *Phys. Lett.* B **433**, 95 (1998).
[5] S. Dimoupoulos and H. Georgi, *Nucl. Phys.* B **193**, 10 (1981).
[6] S. Heinemeyer, et al. hep-ph/0604147; S. Heinemeyer, W. Hollik and G. Weiglein, hep-ph/0412214; A. Djouadi, et al., *Phys. Rev. Lett.* **78**, 3626 (1997).
[7] DØ Collab. (B. Abbott, et al.), *Phys. Rev. Lett.* **82**, 4975 (1999).
[8] DØ Collab., M. Narain, in Div. Part. and Fields Ý92, ed. C. Albright, P. Kasper, R. Raja, J. Yoh, World Scientific (1993).
[9] G. C. Blazey et al., RunII Jet Physics, in Proc. Workshop: QCD and Weak Boson Physics in RunII, eds. U. Bauer, R. K. Ellis, D. Zappenfeld (FERMILAB-PUB-00-297, 2000).
[10] R.H. Dalitz and G.R. Goldstein, *Phys. Rev.* D 45, 1531 (1992).
[11] DØ Collaboration, *Phys. Rev. Letters* 80, 2063 (1998); DØ Collaboration, *Phys. Rev.* D 60, 052001 (1999).
[12] DØ Collaboration, *Phys. Letters* B 655,(2007) 7.
[13] CDF Collab., nuWT analysis in 192 pb-1.
[14] LEP Electroweak Working Group: http://lepewwg.web.cern.ch/LEPEWWG/plots/summer2005.
[15] CDF Collaboration, *Phys. Rev. Lett.* 93, 142001 (2004).
[16] DØ Collaboration, Phys.Lett. B626 (2005) 55.
[17] T. Sjstrand, et al., *Comput. Phys. Commun.* 135 (2001) 238.
[18] M.L. Mangano, et al., *JHEP* 0307 (2003) 001; M.L. Mangano, M. Moretti, R. Pittau, *Nucl. Phys.* B 632 (2002) 343; F. Caravaglios, et al., *Nucl. Phys.* B 539 (1999) 215.
[19] M. Mangano, http://cepa.fnal.gov/patriot/mc4run2/MCTuning/061104/mlm.pdf (2004).
[20] R. Brun, F. Carminati, CERN Program Library Long Writeup (1993) W5013.
[21] V.M. Abazov, *etal.*, "The Upgraded DØ Detector," Fermila b -Pub-05/341-E (2005).
[22] S. Abachi *et al.* [DØ Collaboration], Phys. Rev. D **76**. 052006 (2007).
[23] R. Brun and F. Rademakers, Nucl. Instrum. Meth. A **389**, 81 (1997).
[24] F. James and M. Roos, Comput. Phys. Commun. **10**, 343 (1975).
[25] DØCollaboration "Measurement of Top Quark Mass in the Lepton+Jets Channel using Matrix Element Method," DØ Conf Note 5610.
[26] D Collab. D0-CONF-5747 (2008).